Transient Current in Graphene Transistors Under Single- Proton Irradiation

Wanzhen He
Tsinghua University
ChiYung Yam
Beijing Computational Science Research Center https://orcid.org/0000-0002-3860-2934
Zhiping Xu (xuzhiping@gmail.com)
Tsinghua University https://orcid.org/0000-0002-2833-1966

Article

Keywords: Transient Current, Graphene Transistors, Single- Proton Irradiation, Two-dimensional materials, multilayers, heterostructures

Posted Date: September 2nd, 2021

DOI: https://doi.org/10.21203/rs.3.rs-754114/v1

Transient Current in Graphene Transistors under Single-Proton Irradiation

Wanzhen He[a], Chi-Yung Yam[*,b] and Zhiping Xu[*,a]

[a]*Applied Mechanics Laboratory, Department of Engineering Mechanics, Tsinghua University, Beijing 100084, China*

[b]*Beijing Computational Science Research Center, ZPark II, Beijing 100193, China*

[*]*Email: yamcy@csrc.ac.cn, xuzp@tsinghua.edu.cn*

Two-dimensional materials and their multilayers or heterostructures are promising candidates for optoelectronic devices. Their performance such as the transient current can be remarkably modified under irradiation since the atoms are extremely exposed. This effect, however, still lacks theoretical understanding. Using real-time time-dependent density functional theory extended to open systems for electrons and Ehrenfest dynamics for the moving ion, we explore the single-ion irradiation effects on graphene electronics. Perturbed electronic transport is identified in a field-effect transistor setup. The peak transient current is calculated as the key indicator to quantify the irradiation effects, the irradiation-energy dependence of which shows distinction from the stopping power that was well understood in recent studies. We find that the perturbation in transient current is driven by delocalized plasmonic excitation, in contrast to the localized electronic excitation that has a strong impact on the stopping power. The site dependence of transient current is determined by the local electron density and ionic charge, which highlights the roles of the lattice and elec-

tronic structures of materials. Following these understandings and the database developed for typical space-irradiation conditions, the device responses of graphene nanoelectronics can be modeled. These results and methods lay the ground for the material-informed design of nanoelectronics in, for example, space applications.

Single-particle irradiation (SPI) is the stepping stone to the understanding of ion-matter interaction, which is a crucial issue in irradiation effects concerned in scientific progresses and technological applications, for instance, material modification, imaging, radiation therapy, and space science [1–4]. SPI is also of vital importance in material engineering as seen in the development of focused ion beam, which could implant defects [5] or modify the microstructures [6]. In electronic devices employed in space missions, the single-event effects (SEE) such as single-event upset (SEU) and single-event latch-up (SEL) are examples of radiation events where single ionizing particles penetrate inner nodes, causing errors or damage in electric circuits [2]. For example, the passage of an ion through a field-effect transistor (FET) induces a current transient. Recent proton-radiation experiments on carbon nanotube (CNT) FETs show major and minor SEE signals of $\sim$ 100 nA [7]. Unfortunately, previous studies on SEE rely on analytical models such as diffusion-drift equations [8], where the parameters shift in response to irradiation [9]. The underlying microscopic processes of electronic and lattice excitation, however, are not well understood and have not been implemented in predictive models.

Graphene FETs are promising electronic devices for their superior performance [10]. Irradiation effects of energetic ions on graphene has been investigated [11–14]. Empirical or first-principles

molecular dynamics (MD) simulations with electronic ground states were employed to explore the ion stopping and defect production, which are complex processes determined by the types of projectiles, their kinetic energy and direction of motion, the site of irradiation, and interaction with the substrate. Electronic excitation were captured via real-time time-dependent density functional theory (RT-TDDFT) [15–19], revealing exchange and deposition pathways and processes for both charge and energy. However, all of these studies are limited to the closed systems. The transient current induced in electronic devices, which are open systems that contain two electrodes, and electron flow from (to) the source (drain), remains unexplored in theory, and the rational design of these devices is prohibited.

In this work, we combine RT-TDDFT with the non-equilibrium Green function (NEGF) formalism [20] to treat open electronic systems (TDDFT-OS) [21,22]. This first-principles framework is implemented in the LODESTAR code [21], and used to study single-ion irradiation effects on graphene electronics with an Ehrenfest dynamics approach for the moving ions (**Supplementary Notes 1 and 2**). Charge density wave excitation under ion incidence is analyzed through the time-dependent charge density distribution $\rho(\mathbf{r}, t)$. The peak transient current I_{p} induced during this process and the ion stopping power S are evaluated to be the main indicators in assessing irradiation effects. Their dependence on the energy and site of irradiation are investigated. Based on the obtained map of I_{p}, the device responses in specific irradiation conditions are modeled.

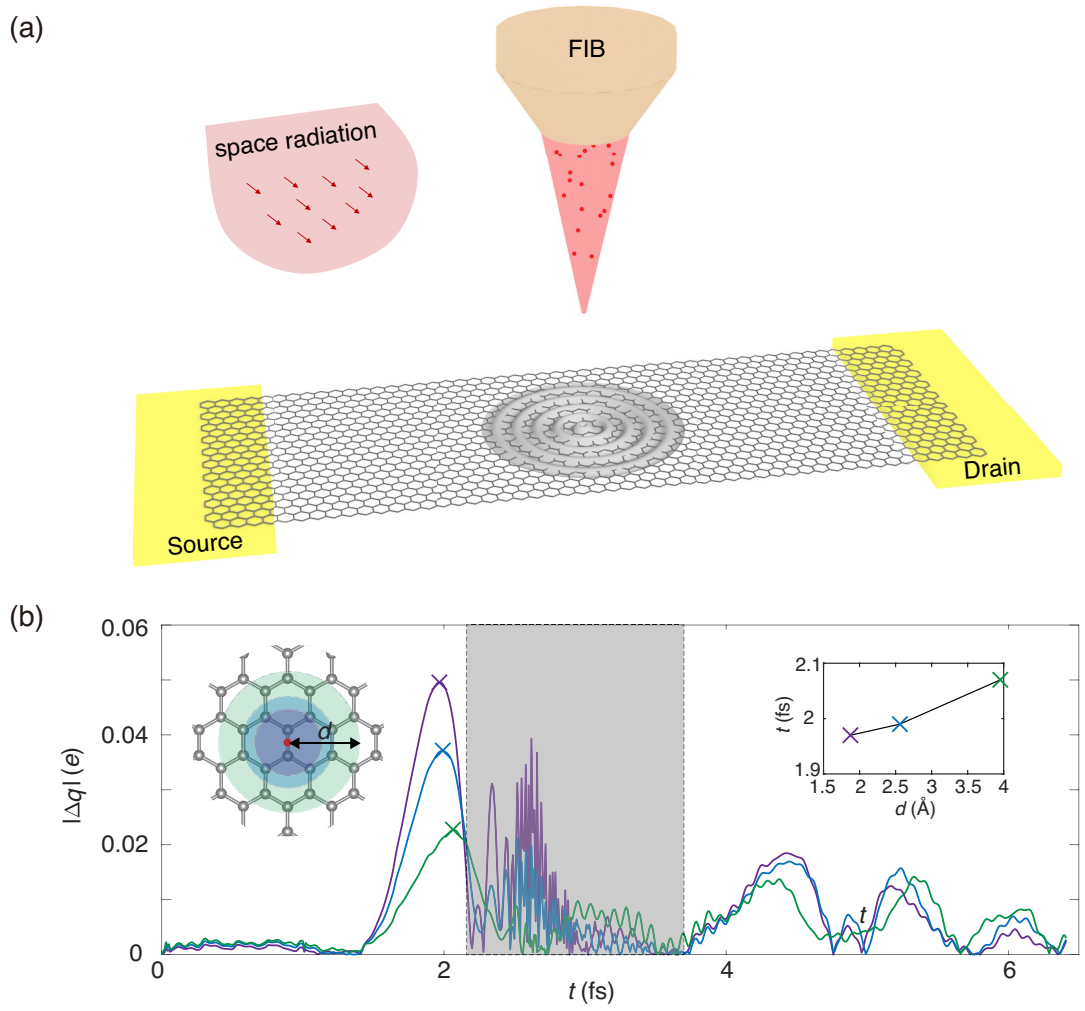

Figure 1 Electronic excitation in graphene electronics under single-ion irraidiation. a. Schematic illustration of charge density waves in a graphene field-effect transistor (FET) under single-H irradiation, from the focused ion beam (FIB) or space radiation, for example. **b.** Changes in the atomic charge ($|\Delta q|$) in area enclosed by a cut-off distance (d) from the site of irradiation (the red dot). The time window for H to pass through the graphene sheet within a thickness of 2 Å is shown in gray. The peak currents I_{p} are marked by crosses. The relation between the time of occurrence t of $|\Delta q_{\max}(t)|$ and the cut-off distance d is plotted as the inset.

RESULTS AND DISCUSSION

The device consists of a lead-scatter-lead setup of a H-terminated zigzag graphene nanoribbon (GNR) (**Figs. 1a** and **S1**). The geometry of scattering region (length 2.0 nm, width 1.4 nm) follows recent experimental realization of graphene FETs [23]. An H atom (the projectile) with a mass of m_{H} is placed 0.4 nm away from the basal plane of graphene initially, and launched with a kinetic (irradiation) energy $K = \frac{1}{2} m_{\mathrm{H}} v_{\mathrm{H}}^2$ or velocity v_{H} at a normal angle of incidence. All atoms in the device are fixed since lattice excitation lags behind electronic processes and contribute less to the perturbation on current in the range of high K values under consideration [16]. Time steps to integrate the RT-TDDFT equations are chosen adaptively between 0.005 and 5 attoseconds for K ranging from 10 eV to 10 MeV, which assure the convergence of simulation results. The bias voltage for all calculations is set to 0.05 V, which is of the same magnitude applied in experiments [7] and previous RT-TDDFT simulations [22,24].

We first analyze the evolution of atomic charges q under a 100-eV H irradiation on bond-center sites in the graphene lattice (**Figs. 1b** and **S1**), which is measured for the transistor in the area within a distance of d from irradiation site. As the H atom passes through graphene within a short window of 2 Å, high-frequency changes are observed for the charge (Δq). The time evolution $\Delta q(t)$ after the ions leave graphene shows damped oscillation, in consistent with our previous RT-TDDFT study using a closed-system approach [16]. The first peak in $|\Delta q(t)|$ corresponds to the maximum value of irradiation-induced change $|\Delta q(t)|_{\max}$ and is identified in the selected region measured by a cut-off distance d. We find that the time of occurrence of $|\Delta q(t)|_{\max}$ increases with

d, suggesting that the single-ion irradiation perturbs the charge density distribution in graphene, resulting in subsequent outward propagation of charge density waves from the site of irradiation. The wave speed is 1.98×10^6 m/s, close to the Fermi velocity in graphene, $v_{\mathrm{F}} = 2.5 \times 10^6$ m/s [25], but one order of magnitude higher than the speed of ionic motion (v_{H}). Therefore, the Born-Oppenheimer approximation would fail at high irradiation energies where electronic excitation becomes significant [16], and the TDDFT-OS scheme should be used for the exploration.

Energy deposition is quantified by the stopping power S. The value of S can be measured by irradiation experiments [26], and is recently shown to be accurately predicted by RT-TDDFT methods to couple the processes of nuclear motion with electronic excitation. RT-TDDFT studies also uncover electron capture and emission events [16,17,19,27]. The response $S(K)$ for graphene displays two peaks at $K =\sim 10$ eV and ~ 1 MeV, which correspond to the nuclear stopping with minor plasmonic electronic excitation [16,17], and rising contributions from electronic stopping [28], respectively. In an open electronic system that is coupled to electrodes, irradiation effects are usually assessed through shift in the current-voltage curve [29] or collected charge at terminals that should not exceed its critical value of (q_{cr}) to avoid device upset [2]. Our simulation results uncover the wave features of plasmonic excitation induced by irradiation (**Fig. 1**), and suggests that the charge deposition is a minor process compared to charge exchange [16]. The discussion is thus focused on the transient current, which is the key quantity to be measured in practice for device performance monitoring.

We choose the peak current I_{p} under perturbation as the main indicator for risk assessment

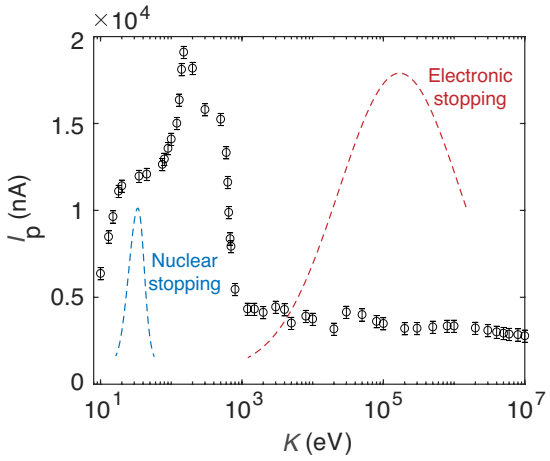

Figure 2 Peak transient current under single-H irradiation on the bond center of graphene. The values of $I_{\rm p}$ under different irradiation energies K, ranging from 10 eV to 10 MeV. The value of $I_{\rm p}$ in absence of irradiation is 350 nA. The dashed curves show the nuclei and electronic stopping powers $S(K)$, the amplitude of which are only for illustration. The peaks are located at ~ 10 eV and ~ 100 keV, respectively.

of device failure (**Fig. 2**). The steady-state current calculated in the absence of ion irradiation is 350 nA, which is close to the value obtained for a GNR FET under the same bias voltage [22]. All results in **Fig. 2** are calculated for H irradiation on the bond-center sites with K ranging from 10 eV to 10 MeV. Energy in this range is sufficiently low to exclude the relativistic effects but high enough to disturb the device, even for a projectile reflected at a relatively low value of $K = 10$ eV. The response $I_{\rm p}(K)$ measured from TDDFT-OS simulations shows a shoulder-peak structure. This feature is very different from that of $S(K)$, and could be explained by the fact that the peak energy $K = 150$ eV is closely tied to the plasmonic excitation in graphene [16]. For $K < 150$ eV, the charge exchange and transfer is limited, while for $K > 150$ eV, the timescale for ion-matter interaction ($\tau \lesssim 1$ fs for ion traveling for 2 Å) is too short to activate sufficient electron exchange through delocalized plasmonic electronic excitation ($\tau \approx 0.3$ fs). For $K \gtrsim 0.1$ MeV, the irradiation process could not even modify the charge state of the projectile (**Fig. S2**), demonstrating the K-independence (**Fig. 2**) of low-dimensional FETs to ultrahigh-energy particle irradiation. The absence of a peak in the MeV range for $I_{\rm p}(K)$ as that in $S(K)$ implies that localized charge excitation contributes to the stopping power but not to the current. These two main irradiation indicators ($I_{\rm p}$ and S) can be evaluated to assess the soft errors and damage for electronics devices, respectively, and verified by future experiments.

The stopping power of materials is usually modeled through atom-based core and bond formula based on atomic compositions. The electronic structure of materials are not explicitly accounted for, and the site-dependence of irradiation effects are not resolved in *the Stopping and Range of Ions in Matter* (SRIM) [26]. However, RT-TDDFT simulations of site-dependent-ion ir-

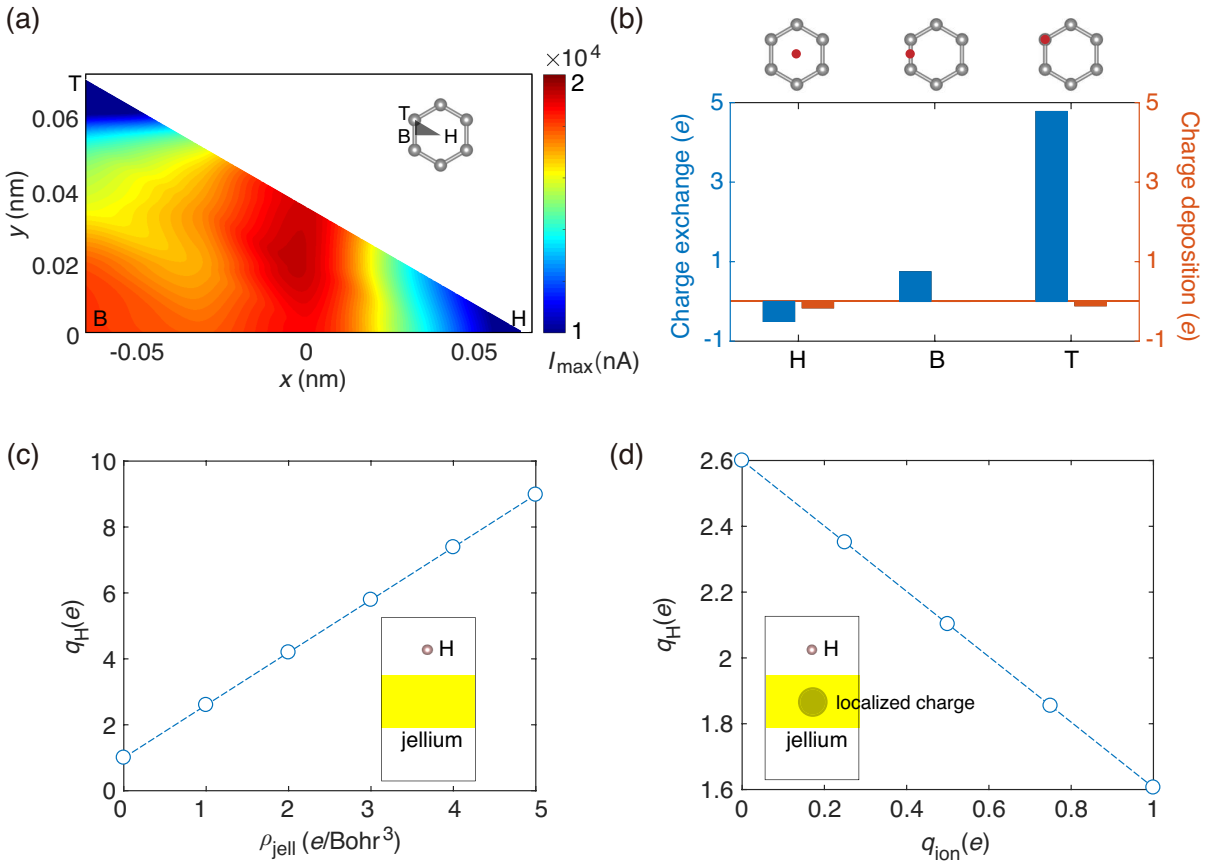

Figure 3 Site dependence of the peak transient current in graphene. a. I_{p} map for irradiation sites sampled in a representative triangle of pristine graphene. The values are calculated at an irradiation energy of $K = 150$ eV and a bias voltage of $V_{\mathrm{b}} = 0.05$ V. **b.** RT-TDDFT calculations of charge exchange and deposition for single-H irradiation on the center of hexagon (H), bond center (B), and the top of atoms (T) in a closed-system approach (**Supplementary Note 2**). **c.** Dependence of charge of hydrogen (q_{H}) on the electron density (ρ_{jell}) in the jellium slab. **d.** Dependence of q_{H} on the charge of ion (q_{ion}) modeled by confined positive charge in a localized sphere with ρ_{jell} = 1 e/Bohr^3.

radiation processes reveal that the energy transfer has a positive correlation with the local charge density [19]. We thus explore the site dependence of I_{p} by extending our previous studies on bond-center irradiation. A map of I_{p} is obtained within a reduced triangular region according to the lattice symmetry (**Fig. 3a**). A uniform grid of sampling is created (**Fig. S3**), and the value of I_{p} is interpolated to the whole area via bi-harmonic splines. We choose $K = 150$ eV that corresponds to the most significant response in I_{p} for the discussion. Statistics show that the induced current ranges from 0.17×10^4 to 1.92×10^4 nA. The responses measured in I_{p} are ranked in the order of bond-center (`B`), top-of-atom (`T`), to center-of-hexagon (`H`) sites, from large to small. This trend can not be directly determined by the knowledge of local charge density, although a positive correlation with the energy deposition (S) or charge exchange was identified for the closed systems [16–18,30] (**Fig. 3b** and **Supplementary Note 2**). On the other hand, charge transfer from graphene to the adsorbed atoms follows a negative order with the local charge density [31]. To clarify the relationship between the site-dependent I_{p} and electronic structures of materials, we explore the effects of electron density and ionic charge using a jellium-slab model with uniformly-distributed electrons [32] using the GPAW code [33]. The results suggest that a higher charge density results in more significant accumulation of electrons with `H` (**Fig. 3c**), while the presence of ionic charges reduces the response through the Coulombic attraction to the electrons (implemented through a confining potential with the same total numbers of electron in the slab, **Fig. 3d**). As a result, I_{p} is small at the `H` site for the low electron density, and at `T` for the presence of a positive `C` ion. In comparison, the site dependence of S originates from the charge density distribution, while that of I_{p} could be modified by the ionic charges.

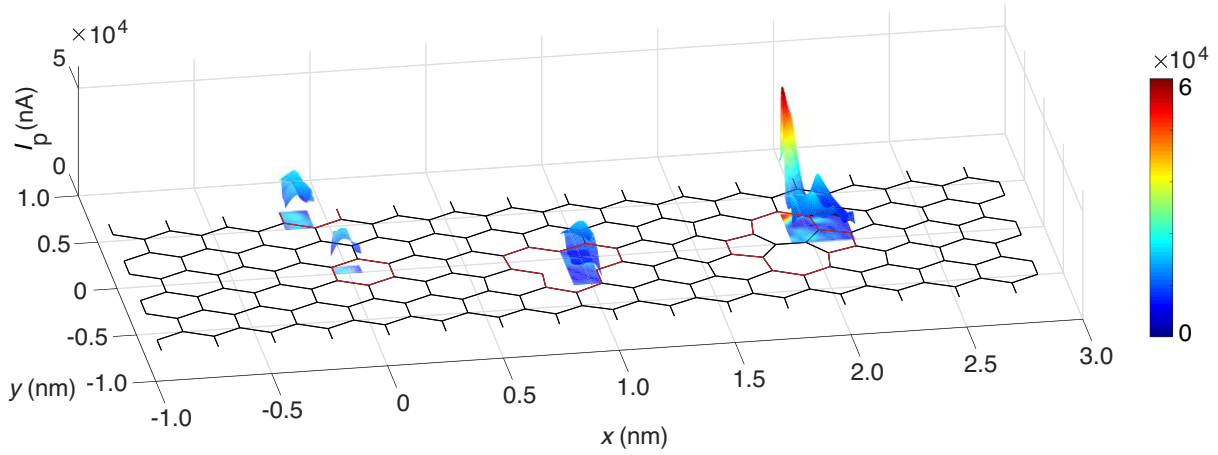

Figure 4 Contour of the peak transient current on pristine and defective sites in graphene. Contour of I_{p} in different regions, including edge, pristine, single vacancy, and Stone-Wales defects from left to right, interpolated from sampling sites in **Fig. S3**. The irradiation energy K is 150 eV, and the bias voltage is V_{b} = 0.05 V.

In graphene FETs, interior and edge defects play a significant role in modulating electronic transport processes [34,35]. The I_{p} map at edges and defect sites (vacancies and Stone-Wales defects) are summarized in **Fig. 4**. In our simulations, the atomic structures are fully relaxed before irradiation, and the irradiation sites are uniformly sampled (**Fig. S3**), followed by interpolation of I_{p}. The results suggest a single-peak feature in the pristine region, at H-terminated edges, and near single vacancies. The strong response at the edges or vacancies could be attributed to the loss of ions. For Stone-Wales defects, multiple peaks are identified for the distorted electronic structures. Therefore, I_{p} in the graphene-based FET is sensitive to both the electronic and lattice structures under single-ion radiation.

The response of a GNR FET can be constructed from our simulation results of pristine

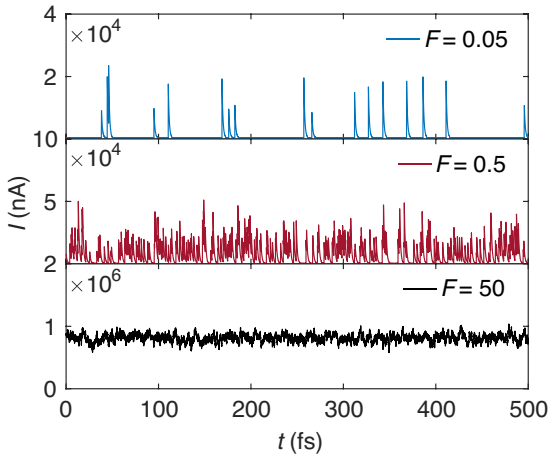

Figure 5 Time-dependent signals in a graphene FET under different irradiation fluxes. Particle irradiation is considered to be uncorrelated events with a damping period of 2 fs based on our TDDFT-OS simulations. Probability of the single irradiation event is determined by the flux F (counts/fs). The perturbed transient current is calculated from the TDDFT-OS simulation results sampled in the pristine graphene (**Fig. 4**). The irradiation energy is $K = 150$ eV, and the current in absence of irradiation is 350 nA under a bias voltage of $V_{\mathrm{b}} = 0.05$ V.

graphene and edge structures (**Fig. S4**). The most significant perturbation from single-H irradiation may result from direct collisions on the path of current flow, including the main path of edges and interior ones connecting carbon atoms in parallel to the edge direction [22]. The I_{p} map for a zigzag-GNR FET indicates that irradiation on the bonds induces significant charge exchange and perturbation on the current. This pathway reveals additional dynamic effects of single-ion irradiation on the electronic devices beyond the knowledge of unperturbed transport properties. With these understandings, we develop a Monte Carlo (MC) algorithm (**Supplementary Note 3** and **Fig. S5**) to simulate the time series of FET signals under an irradiation flux F. We assume that the SPI events are independent, which is a reasonable assumption for the short damping constant of $\tau_{\mathrm{d}} \approx 2$ fs according to our simulation results. The output signal is superposed from the irradiation events. Typical irradiation flux from the proton beams ranges from 10^2 to 10^9 particles/cm^2/s [36], which leads to a maximum of $F \approx 10^{-15}$ counts/fs for a 10^4 nm^2 area. For irradiation by beams with a higher ion flux ($\sim 10^{22}$ particles/cm^2/s, for example [37]), or in extreme space conditions [2], F could increase significantly but still in the SPI regime for nanostructures (the time interval between successive SPI events is much longer than τ_{d}). In our MC simulations at a high flux (**Fig. 5**), the output signal is centered at the current level determined by F with a white-noise feature, while at lower F, discrete changes in the signal of transient current appear either due to single-particle irradiation events on sites with strong responses or superposition of several events. This approach simulates the SEEs in experiments.

CONCLUSIONS

In conclusion, single-particle irradiation processes are modeled in graphene transistors, where outward-propagation of irradiation-induced damped electronic waves is identified in real-time time-dependent density functional theory simulations extended to open electronic systems. The peak transient current is calculated for devices to evaluate potential failure in electric circuits, where the signal is mostly amplified at moderate irradiation energy of 150 eV and is less sensitive to localized electronic excitation compared with stopping power. The dependence of the peak transient current on irradiation sites are mapped, offering a database for the modeling of device responses under specific radiation conditions. The response is shown to be determined by the electron density and ionic charges, which can be modulated from various approaches such as strain, defect and phase engineering that are shown to be prominent for low-dimensional materials [38–40].

References

1. Zhang, H., Miyamoto, Y. & Rubio, A. Ab initio simulation of helium-ion microscopy images: The case of suspended graphene. *Phys. Rev. Lett.* **109**, 265505 (2012).

2. Petersen, E. *Single Event Effects in Aerospace* (John Wiley & Sons, 2011).

3. Li, Z. & Chen, F. Ion beam modification of two-dimensional materials: Characterization, properties, and applications. *Appl. Phys. Rev.* **4**, 011103 (2017).

4. Newhauser, W. D. & Zhang, R. The physics of proton therapy. *Phys. Med. Biol.* **60**, R155 (2015).

5. Malekpour, H. *et al.* Thermal conductivity of graphene with defects induced by electron beam irradiation. *Nanoscale* **8**, 14608–14616 (2016).

6. Willke, P. *et al.* Doping of graphene by low-energy ion beam implantation: Structural, electronic, and transport properties. *Nano Lett.* **15**, 5110–5115 (2015).

7. Bushmaker, A. W. *et al.* Single event effects in carbon nanotube-based field effect transistors under energetic particle radiation. *IEEE Trans. Nucl. Sci.* **61**, 2839–2846 (2014).

8. Zebrev, G. Graphene field effect transistors: Diffusion-drift theory. *Physics and Applications of Graphene: Theory* 480–486 (2011).

9. Zebrev, G. I., Orlov, V. V., Bakerenkov, A. S. & Felitsyn, V. A. Compact modeling of MOSFET I–V characteristics and simulation of dose-dependent drain currents. *IEEE T. Nucl. Sci.* **64**, 2212–2218 (2017).

10. Geim, A. K. & Novoselov, K. S. The rise of graphene. *Nature* **6**, 183–191 (2007).

11. Bai, Z., Zhang, L. & Liu, L. Bombarding graphene with oxygen ions: Combining effects of incident angle and ion energy to control defect generation. *J. Phys. Chem. C* **119**, 26793–26802 (2015).

12. Liu, X. Y., Wang, F. C., Park, H. S. & Wu, H. A. Defecting controllability of bombarding graphene with different energetic atoms via reactive force field model. *J. Appl. Phys.* **114**, 054313 (2013).

13. Shi, T., Peng, Q., Bai, Z., Gao, F. & Jovanovic, I. Proton irradiation of graphene: Insights from atomistic modeling. *Nanoscale* **11**, 20754–20765 (2019).

14. Zhao, S. & Xue, J. Modification of graphene supported on SiO_2 substrate with swift heavy ions from atomistic simulation point. *Carbon* **93**, 169–179 (2015).

15. Lloyd-Hughes, J. *et al.* The 2021 ultrafast spectroscopic probes of condensed matter roadmap. *J Phys. Condens. Matter* **33**, 353001 (2021).

16. He, W., Chen, C. & Xu, Z. Electronic excitation in graphene under single-particle irradiation. *Nanotechnology* **32**, 165702 (2021).

17. Krasheninnikov, A. V., Miyamoto, Y. & Tománek, D. Role of electronic excitations in ion collisions with carbon nanostructures. *Phys. Rev. Lett.* **99**, 016104 (2007).

18. Ojanperä, A., Krasheninnikov, A. V. & Puska, M. Electronic stopping power from first-principles calculations with account for core electron excitations and projectile ionization. *Phys. Rev. B* **89**, 035120 (2014).

19. Vázquez, H. *et al.* Electron cascades and secondary electron emission in graphene under energetic ion irradiation. *Phys. Rev. B* **103**, 224306 (2021).

20. Datta, S. *Quantum Transport: Atom to Transistor* (Cambridge University Press, 2005).

21. Chen, S., Kwok, Y. & Chen, G. Time-dependent density functional theory for open systems and its applications. *Acc. Chem. Res.* **51**, 385–393 (2018).

22. He, S., Russakoff, A., Li, Y. & Varga, K. Time-dependent density-functional theory simulation of local currents in pristine and single-defect zigzag graphene nanoribbons. *J. Appl. Phys.* **120**, 034304 (2016).

23. Wang, X. *et al.* Room-temperature all-semiconducting sub-10-nm graphene nanoribbon field-effect transistors. *Phys. Rev. Lett.* **100**, 206803 (2008).

24. Wen, S. *et al.* Time-dependent current distributions of a two-terminal carbon nanotube-based electronic device. *J. Phys. Chem. B* **115**, 5519–5525 (2011).

25. Hwang, C. *et al.* Fermi velocity engineering in graphene by substrate modification. *Sci. Rep.* **2**, 590 (2012).

26. Ziegler, J. F., Ziegler, M. D. & Biersack, J. P. SRIM: The stopping and range of ions in matter (2010). *Nucl. Instrum. Methods Phys. Res., B* **268**, 1818 (2010).

27. Kononov, A. & Schleife, A. Anomalous stopping and charge transfer in proton-irradiated graphene. *Nano Lett.* **21**, 4816–4822 (2021).

28. Bubin, S., Wang, B., Pantelides, S. & Varga, K. Simulation of high-energy ion collisions with graphene fragments. *Phys. Rev. B* **85**, 235435 (2012).

29. Khanna, V. K. *Extreme-Temperature and Harsh-Environment Electronics* (IOP Publishing Limited Bristol, 2017).

30. Sanville, E., Kenny, S. D., Smith, R. & Henkelman, G. Improved grid-based algorithm for Bader charge allocation. *J. Comp. Chem.* **28**, 899–908 (2007).

31. Moon, H. S., Lee, J. H., Kwon, S., Kim, I. T. & Lee, S. G. Mechanisms of Na adsorption on graphene and graphene oxide: Density functional theory approach. *Carbon Lett.* **16**, 116–120 (2015).

32. Lang, N. & Kohn, W. Theory of metal surfaces: Charge density and surface energy. *Phys. Rev. B* **1**, 4555 (1970).

33. Enkovaara, J. *et al.* Electronic structure calculations with GPAW: A real-space implementation of the projector augmented-wave method. *J. Phys.: Condens. Matter* **22**, 253202 (2010).

34. Orlof, A., Ruseckas, J. & Zozoulenko, I. V. Effect of zigzag and armchair edges on the electronic transport in single-layer and bilayer graphene nanoribbons with defects. *Phys. Rev. B* **88**, 125409 (2013).

35. Shao, J., Pohl, V., Marsoner Steinkasserer, L. E., Paulus, B. & Tremblay, J. C. Electronic current mapping of transport through defective zigzag graphene nanoribbons. *J. Phys. Chem. C* **124**, 23479–23489 (2020).

36. Buchner, S., Marshall, P., Kniffin, S. & LaBel, K. Proton test guideline development: Lessons learned. *NASA Electronic Parts and Packaging Program (NEPP)* (2002).

37. Lee, S. & Saw, S. Plasma focus ion beam fluence and flux: Scaling with stored energy. *Phys. Plasmas* **19**, 112703 (2012).

38. Han, Y. *et al.* Experimental nanomechanics of 2D materials for strain engineering. *Appl. Nanosci.* **11**, 1075–1091 (2021).

39. Lee, S.-M., Kim, J.-H. & Ahn, J.-H. Graphene as a flexible electronic material: Mechanical limitations by defect formation and efforts to overcome. *Mater. Today* **18**, 336–344 (2015).

40. Besse, R. *et al.* Size-induced phase evolution of $MoSe_2$ nanoflakes revealed by density functional theory. *J. Phys. Chem. C* **122**, 20483–20488 (2018).

Supplementary Information

Supplementary Notes S1-S3 Theoretical formalism for the real-time time-dependent density functional theory extended to open systems, the Monte Carlo algorithm, simulation details and charge analysis.

Supplementary Figures S1-S5 Atomic structures of the simulation model, initial and final charge states of hydrogen at different irradiation energies, sampling of pristine and defective sites in graphene, contour of peak current in pristine graphene-nanoribbon field effect transistors, flow chart of the Monte Carlo algorithm to simulate time-dependent current.

Acknowledgements This study was supported by the National Natural Science Foundation of China (11825203, 11832010, 11921002, and 52090032), and the Science Challenge Project through Grant No. TZ2018007. The computation was performed on the Explorer 100 cluster system of Tsinghua National Laboratory for Information Science and Technology.

Author contributions All authors performed the research and wrote the paper.

Competing Interests The authors declare that they have no competing financial interests.

Correspondence Correspondence and requests for materials should be addressed to Z.X. (xuzp@tsinghua.edu.cn).

Data Availability The data that support the plots within this paper and other findings of this study are available from the corresponding author upon reasonable request.

Supplementary Files

This is a list of supplementary files associated with this preprint. Click to download.

- suppinfo.pdf